

Selective skeletal editing of polycyclic arenes using organophotoredox dearomative functionalization

Received: 9 June 2022

Accepted: 19 July 2022

Published online: 05 August 2022

Check for updates

Peng Ji¹, Cassondra C. Davies², Feng Gao¹, Jing Chen¹, Xiang Meng¹,
Kendall N. Houk³✉, Shuming Chen²✉ & Wei Wang¹✉

Reactions that lead to destruction of aromatic ring systems often require harsh conditions and, thus, take place with poor selectivities. Selective partial dearomatization of fused arenes is even more challenging but can be a strategic approach to creating versatile, complex polycyclic frameworks. Herein we describe a general organophotoredox approach for the chemo- and regioselective dearomatization of structurally diverse polycyclic aromatics, including quinolines, isoquinolines, quinoxalines, naphthalenes, anthracenes and phenanthrenes. The success of the method for chemoselective oxidative rupture of aromatic moieties relies on precise manipulation of the electronic nature of the fused polycyclic arenes. Mechanistic studies show that the addition of a hydrogen atom transfer (HAT) agent helps favor the dearomatization pathway over the more thermodynamically downhill aromatization pathway. We show that this strategy can be applied to rapid synthesis of biologically valued targets and late-stage skeletal remodeling en route to complex structures.

Polycyclic scaffolds bearing partially dearomatized fused arenes are commonly encountered in natural products, pharmaceuticals and bioactive molecules^{1–5}. While these molecular frameworks lead to great structural diversity and intriguing biological properties, they engender synthetic challenges as their assembly often requires pre-functionalized substrates and multi-step sequences. Direct dearomatization of fused arenes constitutes an efficient approach for the construction of polycyclic scaffolds due to its high atom and step economy^{1–5}. However, selective dearomatization and functionalization of fused arenes is difficult because harsh conditions are often required to disrupt aromaticity, leading to poor selectivities. As a result, dearomative functionalization of fused arenes has been largely limited to activated arenes such as indoles^{6–15} and naphthols^{16–20}.

Issues of chemo- and regioselectivity also add to the difficulty of dearomative functionalizations of unactivated fused arenes such as quinolines and naphthalenes. Selective dearomatization of pyridine

moieties in fused arenes is feasible^{21–25} owing to the electron deficient nature of pyridine and assistance provided by Lewis acid complexation. Selective dearomatization of phenyl moieties in fused arenes, on the other hand, is significantly more challenging. To our knowledge, only one example has been described in a recent report by Brown, Houk and Glorius involving a photochemical [4 + 2] cycloaddition between quinolines and alkenes (Fig. 1b)²⁶ enabled by energy transfer and Lewis acid activation. A similar [4 + 2] cycloaddition strategy initiated by energy transfer was also employed in the dearomatization of naphthalene by Sarlah et al. (Fig. 1c)^{27–32}.

We wondered if a photoredox strategy could be used to selectively dearomatize the phenyl moieties in quinolines, isoquinolines, quinoxalines, naphthalenes and other fused arenes. In reported photoredox processes, radicals add selectively to the pyridine ring in quinolines^{33,34}, and indiscriminately to the phenyl rings in naphthalenes. In contrast to Sarlah's [4 + 2] cycloaddition

¹Departments of Pharmacology and Toxicology and Chemistry and Biochemistry, University of Arizona, Tucson, AZ 85721-0207, USA. ²Department of Chemistry and Biochemistry, Oberlin College, Oberlin, OH 44074, USA. ³Department of Chemistry and Biochemistry, University of California, Los Angeles, CA 90095-1569, USA. ✉e-mail: houk@chem.ucla.edu; shuming.chen@oberlin.edu; wwang@pharmacy.arizona.edu

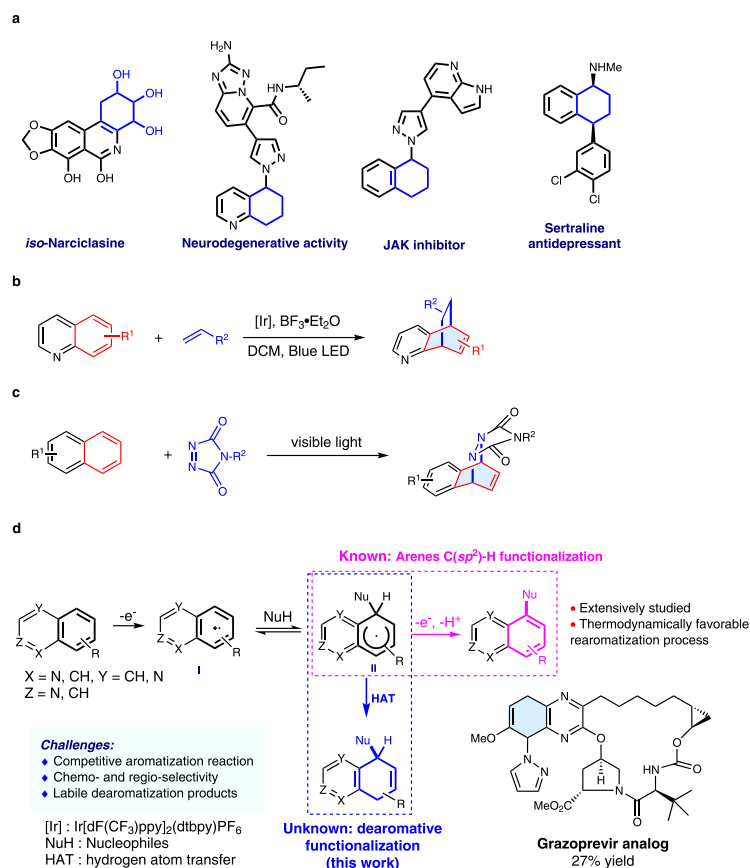


Fig. 1 | Methods for selective dearomative functionalization of fused arenes.

a Examples of partially dearomatic natural products and bioactive compounds.

b Selective dearomatization of quinolines. **c** Selective dearomatization of

naphthalenes. **d** Selective dearomatization of structurally diverse fused arenes (this work).

strategy, in which regioselectivity is governed primarily by steric effects^{27,32}, we envisaged taking advantage of the relative electron richness of the phenyl ring to achieve selective dearomative functionalization (Fig. 1d). Photocatalytically promoted single electron transfer (SET) oxidation of quinolines would produce radical cation **I**, in which the positive charge is mostly localized on the phenyl ring. We anticipated nucleophiles to add to intermediate **I** selectively to form radical **II**. Direct arene C(sp²)-H functionalization with nucleophiles under photoredox catalysis or electrophotocatalysis conditions have been elegantly leveraged by Nicewicz^{35–38}, Lambert³⁹, Hu⁴⁰, and Wickens⁴¹ to generate aromatic functionalized products. We postulated that it would be possible to direct the reaction toward the less thermodynamically stable dearomatized products by capturing radical **II** with a sufficiently activated hydrogen atom transfer (HAT) agent.

In this work, we describe the successful development of a general chemo- and regioselective method for the dearomative functionalization of diverse fused arenes using this strategy.

Results and discussion

Reaction model design

In order to undergo selective photoredox promoted dearomative functionalization, fused arenes must have oxidation potentials that enable them to be oxidized by excited states of photocatalysts (PCs) through SET. The oxidation potential of unsubstituted quinoline ($E^{\text{ox}} = 2.23 \text{ V vs SCE}$, Supplementary Fig. 2) suggests that its oxidation would be very difficult using common PCs. However, introduction of an OMe group onto the phenyl moiety of quinoline lowers the oxidation potential sufficiently (e.g., 6-methoxyquinoline **1a**, $E^{\text{ox}} = 1.83 \text{ V vs SCE}$, Table 1 and Supplementary Fig. 2), making it possible to

participate in thermodynamically driven SETs with excited states of conventional organophotoredox catalysts such as acridinium and triphenylpyrylium (TPT) salts that have excited state reduction potentials (E^{red}) greater than 2.0 V (Table 1).

Reaction optimization

We assessed the viability of the proposed dearomative functionalization protocol by reacting 6-methoxyquinoline **1a** with pyrazole **2a** as a nucleophile under irradiation with blue LEDs in DCM solution containing HAT agents and commercially available organic photosensitizers (Table 1). The desired dearomatization product **3a** is generated in the highest yield using 1.5 equiv of **1a**, 1.0 equiv of **2a** (0.05 M), 2.5 mol% *N*-phenylmeso-acridinium tetrafluoroborate (**Mes-Acr2**), and 0.2 equiv of the HAT agent. Nucleophile addition occurred exclusively at the 5-position. The efficiency of the reaction is dependent on the HAT agent (Supplementary Table 1). Among the 17 different thiols and benzeneselenols screened, Ph₃SiSH was found to be the superior HAT agent, leading to regioselective formation of **3a** in 81% yield (Table 1, entry 1). While photocatalysts such as **TPT** ($E^{\text{red}} = 2.55 \text{ V vs SCE}$, 18%, entry 4) with excited state reduction potentials higher than the oxidation potential of **1a** were found to promote this reaction, **Mes-Acr2** (2.5 mol%, $E^{\text{red}} = 2.2 \text{ V vs SCE}$) was identified as the best photocatalyst (**3a** formed 81% ¹H NMR yield, entry 1). Solvent has a significant effect on the reaction (Supplementary Table 2). Furthermore, substrate ratio (Supplementary Table 3) and concentration have a marked impact on the yield (entries 7–11) with low concentrations of **1a** being more beneficial (entries 7 vs 10). The absence of 2,6-lutidine does not affect the reaction outcome (entries 1 vs 10) as quinoline **1a** can serve as the base. Lastly, control experiments confirm that the HAT agent, light and photocatalyst are all required for selective

Table 1 | Exploration and optimization of reaction conditions

"Standard Conditions"
Mes-Acr2 (2.5 mol%)
 Ph_3SiSH (0.2 equiv)
 DCM (0.05 M)
 40 W Blue LEDs, N_2 , rt, 48 h

1a (1.5 equiv) + **2a** (1.0 equiv) $\xrightarrow{\text{Standard Conditions}}$ **3a** + **4a**

$E^{\text{ox}} = 1.83 \text{ V vs SCE}$

Mes-Acr1: $\text{R}^1 = \text{Me}$, $\text{R}^2 = \text{H}$ ($E^{\text{red}} = 2.06 \text{ V vs SCE}$)

Mes-Acr2: $\text{R}^1 = \text{Ph}$, $\text{R}^2 = \text{H}$ ($E^{\text{red}} = 2.20 \text{ V vs SCE}$)

Mes-Acr3: $\text{R}^1 = \text{Ph}$, $\text{R}^2 = \text{Me}$, ($E^{\text{red}} = 2.09 \text{ V vs SCE}$)

TPT
($E^{\text{red}} = 2.55 \text{ V vs SCE}$)

DCA
($E^{\text{red}} = 1.99 \text{ V vs SCE}$)

4CzIPN
($E^{\text{red}} = 1.35 \text{ V vs SCE}$)

Entry	Variation from the "Standard Conditions" ^a	Yield ^b (%)
1	None	81, 76 ^c (<5 of 4a) ^b
2	Mes-Acr1 instead of Mes-Acr2	75
3	Mes-Acr3 instead of Mes-Acr2	67
4	DCA instead of Mes-Acr2	34
5	TPT instead of Mes-Acr2	18
6	4CzIPN instead of Mes-Acr2	trace
7	DCM (0.5 M) with 2,6-lutidine (0.2 equiv)	20
8	DCM (0.2 M) with 2,6-lutidine (0.2 equiv)	49
9	DCM (0.1 M) with 2,6-lutidine (0.2 equiv)	63
10	DCM (0.05 M) with 2,6-lutidine (0.2 equiv)	76
11	DCM (0.025 M) with 2,6-lutidine (0.2 equiv)	74
12	without Ph_3SiSH	53 (23 of 4a) ^b
13	without Mes-Acr2	trace
14	without light	trace
15	390 nm light	40
16	O_2 instead of N_2	trace (56 of 4a) ^b

^aStandard conditions: unless otherwise specified, a mixture of 6-methoxyquinoline **1a** (0.3 mmol, 0.05 M), pyrazole **2a** (0.2 mmol), Ph_3SiSH (0.04 mmol), and **Mes-Acr2** (0.005 mmol) in DCM under a N_2 atmosphere at room temperature was irradiated with 40 W Kessil blue LEDs for 48 h.

^bYield determined by ^1H NMR spectroscopy using 1,3,5-trimethoxybenzene as an internal standard.

^cIsolated yield.

dearomatization. In particular, the HAT agent is critical for minimizing the formation of the aromatization product **4a** (entries 1 vs 12).

Dearomatization of quinolines, isoquinolines, and quinoxalines.

Having established optimal conditions for the photoredox promoted dearomative functionalization reaction, we next explored the scope with fused arenes as substrates and azoles as nucleophiles (Fig. 2a). Our results show that the reaction proceeds with high chemo- and regioselectivity for a wide range of quinolines and azoles. Both electron-donating (**3f**, **3m**) and electron-withdrawing groups are tolerated on the pyrazole. Halogenated pyrazoles reacted with 6-methoxyquinoline with Ph_3SiSH as the HAT agent (condition A giving **3b–3d**). For 5-fluoropyrazole, benzeneselenol, which is 10-fold more reactive than thiols in HAT^{42,43}, is required along with 2,6-lutidine (condition B) to yield **3e**. Other electron-deficient pyrazoles also reacted in the presence of benzeneselenol to produce **3h** and **3i** (condition C, without 2,6-lutidine). Notably, the dearomatization method can be applied to a pyrazole boronate, which generates **3j** (73%) containing a useful handle for subsequent coupling reactions.

Di- and trisubstituted pyrazoles also reacted smoothly to form **3k** (51%) and **3l** (69%), as did other common azoles including benzotriazole (**3n**), 1,2,3-triazoles (**3o**), and tetrazole (**3p**) under condition B or C. Alkyl amines are also good nucleophiles for the dearomatization of quinolines, generating **3q** (40%) and **3r** (35%).

6-Alkoxy-substituted quinolines are particularly effective substrates for the dearomative functionalization reaction, producing diverse substituted 5,8-dihydroquinolines as products (Fig. 2a). A wide range of alkoxy substituents, including those containing methyl/ethyl (**3s**, **3u**, **3v**, and **3z**), ester (**3t**, **3am**), bromo (**3x**), amide (**3w**), phthalimide (**3aa**), alkene (**3ab**), benzyl (**3ac**, **3ad**), TBS (**3ae**, **3af**), MOM (**3ag**), phenyl (**3ah**), ketone (**3ai**), alkyne (**3an**), nitrile (**3ac**, **3ao**), thiophene (**3aj**) and benzofuran (**3al**) moieties, are well tolerated. Moreover, the process promotes selective dearomatization and functionalization of quinoline ring systems even when other arene moieties including benzene (**3q**, **3aa**, **3ac**, **3ad**, **3ah**, **3ai**), thiophene (**3r**, **3aj**) and benzofuran (**3al**) are present. Notably, the protocol enables highly selective dearomatization of a quinoline ($E^{\text{ox}} = 1.86 \text{ V vs SCE}$) over a naphthalene ($E^{\text{ox}} = 1.92 \text{ V vs SCE}$) ring (**3ak**) despite their similar oxidation

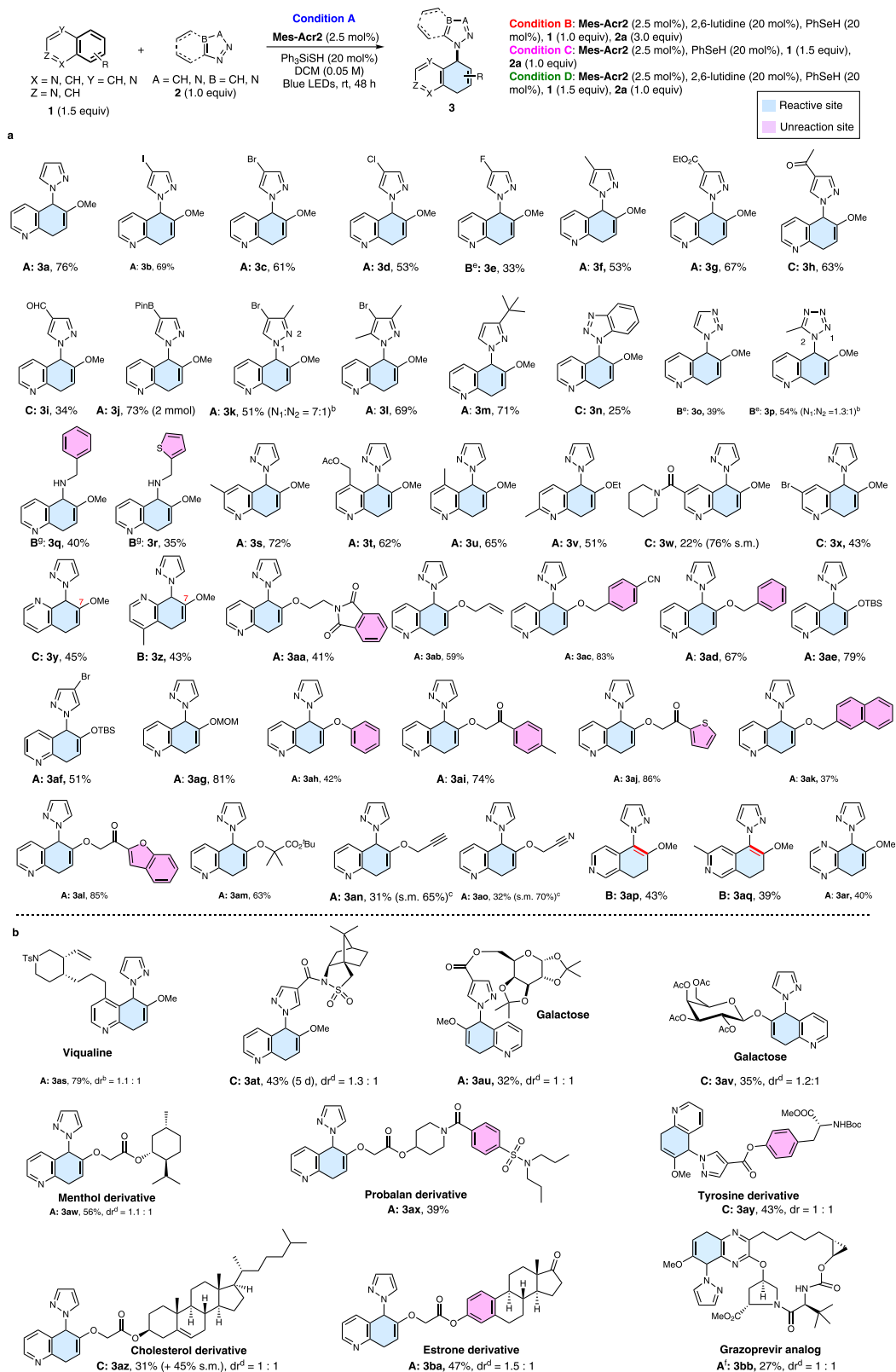


Fig. 2 | Scope of photoredox dearomative functionalization of quinolines, isoquinolines, and quinoxalines with azoles. a Scope of quinolines and quinoxalines with azoles. **b** Late-stage functionalization. ^aReaction conditions: unless otherwise specified, see footnote a of Table 1 and supplementary information; ^bRatio of isomers was determined by using ¹H NMR analysis of the crude reaction

mixture; ^cs.m.: starting materials; ^ddr value was determined by ¹H NMR analysis of the crude reaction mixture; ^eCondition B without 2,6-lutidine; ^fCondition A using 3,6-di-*tert*-butyl-9-mesityl-10-phenylacridin-10-ium tetrafluoroborate as photocatalyst for 5 d. ^gCondition B but using amines (2.0 equiv) and 3,6-di-*tert*-butyl-9-mesityl-10-phenylacridin-10-ium tetrafluoroborate as photocatalyst for 2 d.

potentials. In addition to controlling chemoselectivity, 6-alkoxy groups also direct site selective formation of 5-nucleophile-substituted-5,8-dihydroquinolines. Furthermore, dearomatization of 7-methoxyquinolines is also highly regioselective generating only 8-substituted 5,8-dihydroquinoline products (**3y**, **3z**). Isoquinolines can participate in the process (**3ap**, **3aq**). However, regioisomeric 7,8-dihydroisoquinolines are formed. Finally, quinoxalines are also viable substrate for the dearomatization process (**3ar**).

Owing to the mild conditions required, the organophotoredox-promoted dearomative functionalization process is applicable to late-stage functionalizations of complex pharmaceutically relevant quinoline structures including viqualine (**3as**), Oppolzer's camphorsultam (**3at**), galactose (**3au**, **3av**), menthol (**3aw**), probalan (**3ax**), tyrosine (**3ay**), cholesterol (**3az**), and estrone (**3ba**) groups (Fig. 2b). It is particularly impressive that a grazoprevir analog (**3bb**) containing various functional groups was selectively dearomatized utilizing this process. These results underscore the mildness, high chemo- and regioselectivity, and practicality of this protocol.

Dearomatization of fused arenes. Encouraged by the success of the photoredox reaction of quinolines, we explored its utility for the selective dearomatization of fused non-heteroaromatics. The results show that selective dearomatization of fused arenes is more challenging. As with quinolines, electron-donating substituents can be used to lower the oxidation potentials and enhance reactivity. A 2-methoxy substituent in naphthalene, for instance, lowers the oxidation potential to 1.8 V (vs SCE, supplementary Fig. 2) and enables selective oxidation by the excited state of photocatalyst **Mes-Acr2**. Selective dearomatization and C-1 functionalization of 2-methoxynaphthalene by pyrazole using condition B led to **3bc** (Fig. 3a). The efficiency of this process is also dependent on the base and the HAT agent, as are shown in **3bd**, **3be**, and **3bm** (condition C), **3bf**, **3bj**, **3bk**, **3bl**, and **3bn** (condition B) and **3bi** (condition D). The dearomatization strategy can be applied to methyl substituted naphthalene (**3bg**). Finally, unsubstituted naphthalene (**3bh**) also participates in the process to produce the 1-substituted product regioselectively.

UV-mediated photochemical dearomative functionalization of naphthalene and phenanthrene with excess amines and cyanide (10–25 equiv) were reported by Yasuda and Pac in 1970s and 80s^{44–47}. However, these classic methods showed very limited substrate scopes and poor functional group tolerance due to the harsh activation method. Furthermore, it is challenging to employ these methods for dearomatization of fused heteroaromatic systems such as quinoline, isoquinoline, and quinoxaline because they cannot be activated by UV light. In contrast, our mild, visible-light-mediated photoredox reaction can be applied to the dearomative functionalization of polycyclic aromatic hydrocarbons with a broad substrate scope, in addition to highly-valued fused heteroaromatics. High yields with azoles, which are challenging nucleophiles in Yasuda and Pac's UV method, are obtained for simple anthracene (**3bo**, 87%) and phenanthrene (**3bp**, 73%) (Fig. 3b). Notably, 6-methoxyphenanthrene reacts to form the *trans* substitution product **3bq** (84%). Moreover, nucleophiles other than azoles, such as trifluoromethanesulfonamide (**3br**) and imidazole (**3bs**), can also participate in the process. Furthermore, carboxylic acids, which are often used as radical precursors in photoredox reactions⁴⁸, serve as effective nucleophiles for dearomative functionalization of phenanthrenes. These reactions proceed in moderate to high yields (**3bt–3cf**, 25–89%) and display broad functional group tolerance including phenyl (**3bv**, **3bx**), azide (**3bw**), alkenyl (**3by**), alkynyl (**3bz**), cyclobutyl (**3ca**), and hydroxyl acid groups (**3cf**). Due to their weaker nucleophilicity and steric effects, benzoic acid (**3cb**) and secondary carboxylic acids (**3ca**) are less effective nucleophiles for this process. In addition, the reaction can be utilized for the direct modification of biologically relevant structures such as aspirin (**3cb**) and amino acids (**3cc–3ce**).

Synthetic applications

Studies with the silyloxyquinoline **1b** show that the synthetic protocol can be scaled up without loss of yield (Fig. 3c). Moreover, the reaction can be adapted for use in a flow system, an emerging technology in organic synthesis⁴⁹. Using the flow system, the reaction time is reduced dramatically to 3 h without compromising the yield. The product silylenol ether **3ae** can be converted to the corresponding alcohol **3cg**. The preparative power of this method was also demonstrated by its use in the cost-effective synthesis of important biologically active targets, including a JAK inhibitor (Fig. 3d)⁵⁰. Our synthetic route starts from naphthalene (\$0.04/g) instead of the more expensive 1-bromo-1,2,3,4-tetrahydronaphthalene (\$370/g) used in the earlier preparative pathway⁵⁰. Dearomatization of naphthalene with pyrazol-4-ylboronic acid pinacol ester produces key intermediate **3ch**, which is then reduced using Rh/Al₂O₃ catalyzed hydrogenation to form **3ci**. The JAK inhibitor is then readily prepared from **3ci** using reported procedures⁵⁰. For synthesis of the compound with neurodegenerative activity shown in Fig. 3d, our protocol employed 6-hydroxyquinoline (\$1.6/g) as starting material, which is much cheaper than the previously used precursor, 5-hydroxy-5,6,7,8-tetrahydroquinoline (\$416/g)⁵¹. These studies clearly demonstrate the synthetic value of the our dearomative functionalization protocol, which provides direct and efficient access to polycyclic partially dearomatized frameworks that were previously inaccessible or required strenuous synthetic efforts.

Mechanistic studies. To gain insight into the reaction mechanism, we conducted additional experimental and computational studies. The excited state PC^{•+} **Mes-Acr2**^{*} possesses strong oxidizing power ($E^{\text{red*}} = 2.2$ V) and can oxidize the 6-methoxyquinoline (**1a**) ($E^{\text{ox}} = 1.83$ V vs SCE, supplementary Fig. 2) to give radical cation **5a** (Fig. 4a and Stern-Volmer quenching experiments, supplementary Figs. 3 and 4). The oxidation potential of the fused arene substrate is crucial for the success of this process, as demonstrated by the high reactivity of **1a** in contrast to the lack of reactivity of unsubstituted quinoline ($E^{\text{ox}} = 2.23$ V vs SCE, Supplementary Fig. 2). In addition, when a mixture of **1a** and 6-acetoxyquinoline (**1c**) ($E^{\text{ox}} = 2.2$ V vs SCE, supplementary Fig. 2) is subjected to the reaction conditions, only **1a** undergoes selective dearomatization to form **3a**, indicating that electron-withdrawing substituents inhibit the reaction. In contrast, **1a** and 2-methoxynaphthalene (**1e**, $E^{\text{ox}} = 1.8$ V vs SCE, Supplementary Fig. 2), which have similar oxidation potentials, both react under the same conditions to produce the corresponding dearomatized products **3a** and **3bc** (Fig. 4b). Likewise, phenanthrene **1d** ($E^{\text{ox}} = 1.91$ V vs SCE, Supplementary Fig. 2) is an effective substrate for this process (Fig. 4b). Notably, the pyrazole nucleophile ($E^{\text{ox}} = 2.15$ V vs SCE, Supplementary Fig. 2) is not oxidized by **Mes-Acr2**^{*}. This is supported by luminescence quenching study of **Mes-Acr2** with varying concentrations of 6-methoxyquinoline **1a** and pyrazole **2a** (Supplementary Fig. 4).

Following the oxidation of **1a** through SET, pyrazole reacts with the electrophilic radical cation **5a** to form the radical cation **6a** (Fig. 4a). Calculated Hirshfeld charge and spin densities (Fig. 5a; see Supplementary Fig. 6 for calculated charge and spin densities for other substrates) indicate that C5 has the highest spin density (bold face) in **5a** and is therefore the preferred site for nucleophilic addition. The calculated free energies of the key transition states also support the observation that pyrazole attack at the C5 position is kinetically favored over C8 or C7 by at least 3 kcal/mol (Fig. 5b).

Subsequent exothermic deprotonation of **6a** by 2,6-lutidine gives a neutral radical **7a** (Fig. 5c). Calculated free energies suggest that sequential SET oxidation and deprotonation of **7a** to form the aromatic substitution product **4a** is more thermodynamically favorable (–62.5 kcal/mol from **7a** with the excited state PC^{•+} **Mes-Acr2**^{*} as the oxidant, Figs. 5c and S7). This is reflected in the outcomes of processes

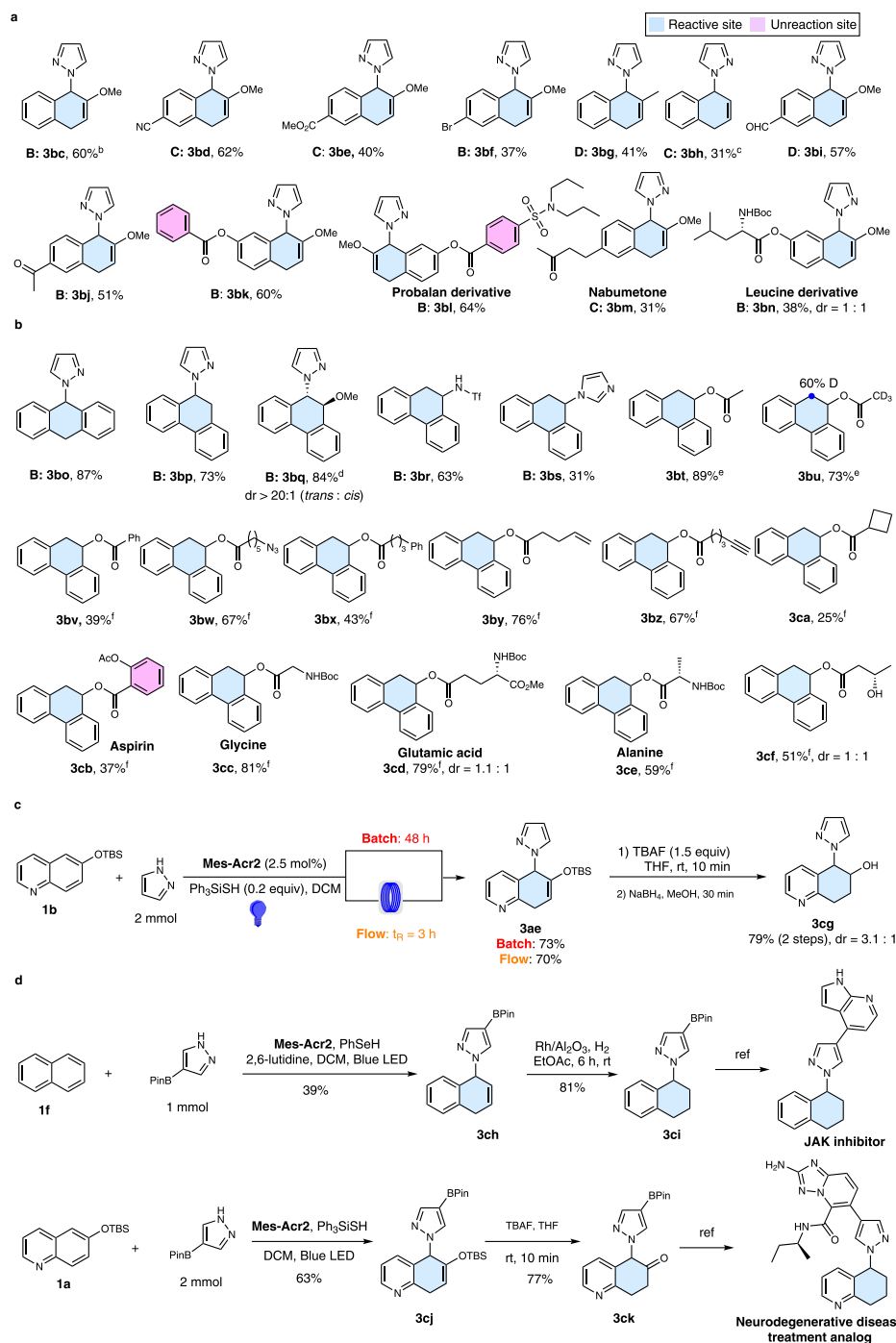


Fig. 3 | Dearomatization of fused arenes. a Scope of naphthalenes. **b** Scope of anthracenes and phenanthrenes. **c** Large scale synthesis. **d** Application in synthesis of valuable targets. ^aReaction condition: unless specified, see footnote a of Table 1

and the ESI; ^bRatio of 6-methoxynaphthalene to pyrazole is 1: 2; ^cRatio of naphthalene to pyrazole is 2:1; ^dReaction time: 4 d; ^eCondition B using 10.0 equiv of acid; ^fCondition B using 5.0 equiv of acid.

leading to fully aromatic products developed by Nicewicz^{35–38}, Lambert³⁹, Hu⁴⁰ and Wickens⁴¹. However, the aromatization pathway requires an oxidant (such as the excited-state photocatalyst or oxygen) to be present in sustained concentrations. Because this pathway does not regenerate the photocatalyst, the aromatization process has been previously noted to be slow in the absence of oxygen, despite its favorable thermodynamics.

Given the apparent hurdles in the aromatization pathway, we reasoned that the presence of a reactive HAT agent (e.g., Ph₃SiSH) could intercept **7a** and redirect the course of the reaction toward the dearomatized product **3a** rather than the more stable aromatic

product **4a** (Fig. 5c). We elected to employ thiol and selenol HAT agents that have weak S-H and Se-H bonds (S-H: 82 kcal/mol, Se-H: 73 kcal/mol) and correspondingly high H-atom transfer rates (PhSH: $K_{20} = 9.0 \times 10^7 \text{ M}^{-1} \text{ s}^{-1}$ and PhSeH: $K_{20} = 1.3 \times 10^9 \text{ M}^{-1} \text{ s}^{-1}$)^{42,43,52}. Indeed, the addition of the HAT agent had a marked effect on the yield of the dearomatized product. Control experiments showed that in the absence of the HAT agent Ph₃SiSH, the yield of the dearomatized product **3ae** dropped from 76% to 31% (Fig. 4c). The effect of the HAT agent is particularly noticeable in reactions of isoquinolines and naphthalenes with pyrazole. Only when PhSeH is present do these processes produce the desired products **3ap** and **3bc** (Fig. 4c). In these

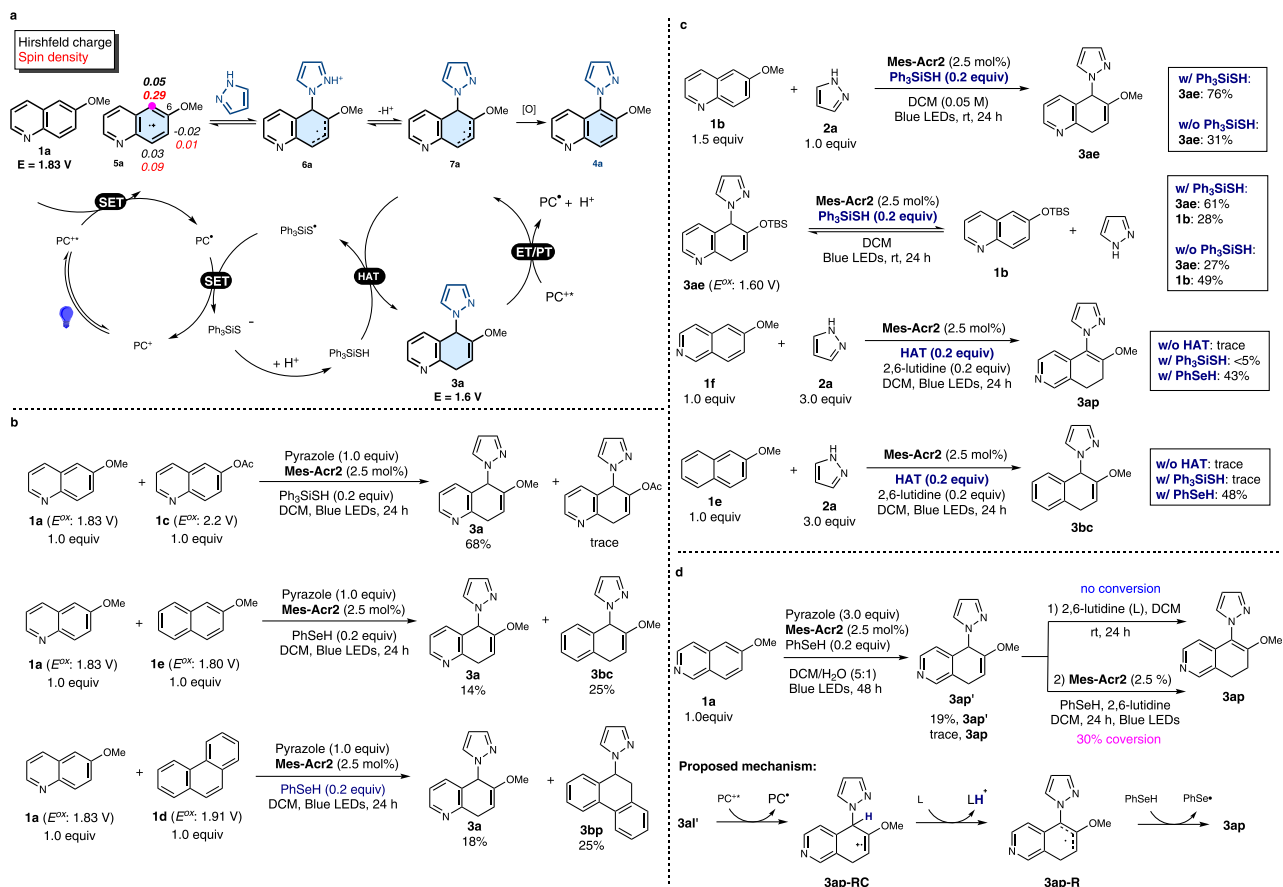


Fig. 4 | Mechanistic studies. a Proposed catalytic cycle. **b** Chemoselectivity studies. **c** Study of roles of HAT reagent. **d** Study of regioselectivity of isoquinoline engaged reaction.

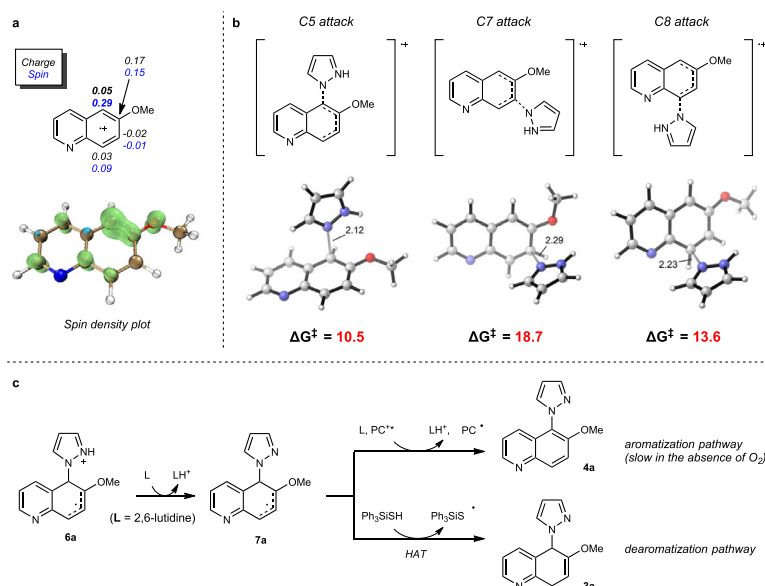


Fig. 5 | Computational investigations. a Calculated Hirshfeld charge and spin densities of radical cation **5a** at the ω B97X-D/def2-TZVPP, SMD (CH_2Cl_2)// ω B97X-D/def2-SVP level of theory. Free energies are in kcal/mol, and interatomic distances are in Å. **b** Calculated C–N forming transition states for the reaction

between **5a** and pyrazole at the ω B97X-D/def2-TZVPP, SMD (CH_2Cl_2)// ω B97X-D/def2-SVP level of theory. Free energies are in kcal/mol, and interatomic distances are in Å. **c** Possible fates of radical cation **6a**.

cases, the HAT process might have been further facilitated by the polarity match⁴⁸ between the protic S-H/Se-H and the nucleophilic carbon radical **7a**. Calculations on the HAT step also confirm that PhSeH decreases the barrier of the HAT step by about 9 kcal/mol

relative to Ph₃SiSH (Supplementary Fig. 7). After the HAT step, the Ph₃SiS• radical is reduced to the Ph₃SiS⁻ anion by the PC• Mes-Acr2 radical. Protonation of the Ph₃SiS⁻ anion regenerates both the HAT agent Ph₃SiSH and the ground-state photocatalyst Mes-Acr2 (Fig. 4a).

Further computational efforts are underway in our laboratories to elucidate the full mechanistic picture (see discussion accompanying Supplementary Fig. 8).

In addition to promoting the formation of the dearomatized product **3a**, the HAT agent Ph₃SiSH also retards the conversion of **3a** ($E^{ox} = 1.60$ V vs SCE, Supplementary Fig. 2) back to the starting material **1a** via PC⁺(Mes-Acr2⁺)-mediated oxidation under the standard reaction conditions (Fig. 4c). Specifically, preliminary experiments show that the photoinduced reaction of **3a** in the presence of Ph₃SiSH leads to 61% recovery of **3ae** and formation of 28% of **1b**. In contrast, in the absence of the HAT agent, **1b** was produced in 49% yield.

It is also worth noting that the dearomatization pathway selectively produced the 5,8-dihydroquinoline regioisomer **3a**. We did not observe the formation of the 7,8-dihydroquinoline **3a'**, which was calculated to be 3.8 kcal/mol less stable than **3a** due to the steric repulsion between the alkene substituents (Supplementary Fig. 8). However, reactions between isoquinolines and pyrazole yielded the regioisomeric 7,8-dihydroisoquinolines. Our experiments suggest that the reaction initially forms 5,8-dihydroisoquinoline **3ap'**, which is then converted to the more stable 7,8-dihydroisoquinoline **3ap** (Fig. 4d). The 5,8-dihydroisoquinoline **3ap'** was obtained in the presence of H₂O. Two possible pathways could lead to 5,8-dihydroisoquinoline **3ap**. The deprotonation/C=C isomerization pathway was ruled out as we did not observe the formation of **3ap** when **3ap'** was treated with 2,6-lutidine, a base used in the dearomatization process. In contrast, **3ap** was formed under the photoredox reaction conditions through SET oxidation of the C=C bond, deprotonation and HAT processes. This pathway was also supported by calculated reaction energies (Supplementary Scheme 1).

In this work, we develop a conceptually unique organophotoredox catalytic dearomative functionalization strategy for the selective disruption of aromaticity in fused arenes. A reactive HAT agent is utilized to help direct the reaction toward the dearomatized product over the thermodynamically more favorable aromatized product. The preparative power of the protocol is demonstrated by applications to structurally diverse fused arenes including quinolines, isoquinolines, quinoxalines, naphthalenes, anthracenes and phenanthrenes. The method can also be applied to the synthesis and late-stage skeletal editing of complex pharmaceutically valued structures. We anticipate that this process will enable facile access to a wide range of synthetically versatile frameworks and accelerate the construction of new molecular architectures for drug discovery.

Methods

Representative procedures for the dearomatization of heteroarenes

To an oven-dried 20 mL-Schlenk tube equipped with a stir bar, was added pyrazole (0.2 mmol), quinoline derivatives (0.3 mmol), Ph₃SiSH (0.04 mmol), and Mes-Acr2 (0.005 mmol). The tube was evacuated and back-filled with N₂ for three times, then sealed with rubber stopper and parafilm. Subsequently, the degassed dichloromethane (4 mL) was added. The reaction was irradiated by the two 40 W Kessil Blue LEDs, cooling by the electronic fan. After the completion of reactions (usually 48 h), the resulted solution was purified by flash column chromatography on silica gel eluting with hexane/ethyl acetate or DCM/ethyl acetate in indicated ratio.

Representative procedures for the dearomatization of arenes

To an oven-dried 20 mL-Schlenk tube equipped with a stir bar, was added pyrazole (0.6 mmol), naphthalene derivatives (0.2 mmol), PhSeH (0.04 mmol), Mes-Acr2 (0.005 mmol), 2,6-lutidine (0.04 mmol) as the base, will be added. The tube was evacuated and back-filled with N₂ for three times, then sealed with rubber stopper and parafilm. Subsequently, the degassed dichloromethane (4 mL) was added. The reaction was irradiated by the two 40 W Kessil Blue LEDs,

cooling by the electronic fan. After the completion of reactions, the resulted solution was purified by flash column chromatography on silica gel eluting with hexane/ethyl acetate or DCM/ethyl acetate in the indicated ratio.

Data availability

Experimental procedures and characterization data are given in the Supplementary Information. The authors declare that all other data supporting the findings of this study are available within the article and its Supplementary Information files. For Cartesian coordinates, see Supplementary Data 1 file. Further data can be obtained from the corresponding author upon request.

References

- Pape, A. R., Kaliappan, K. P. & Kündig, E. P. Transition-metal-mediated dearomatization reactions. *Chem. Rev.* **100**, 2917–2940 (2000).
- López Ortiz, F., Iglesias, M. J., Fernández, I., Andújar Sánchez, C. M. & Ruiz Gómez, G. Nucleophilic dearomatizing (DNAr) reactions of aromatic C-H systems. A mature paradigm in organic synthesis. *Chem. Rev.* **107**, 1580–1691 (2007).
- Roche, S. P. & Porco, J. A. Dearomatization strategies in the synthesis of complex natural products. *Angew. Chem. Int. Ed.* **50**, 4068–4093 (2011).
- Zheng, C. & You, S.-L. Advances in catalytic asymmetric dearomatization. *ACS Cent. Sci.* **7**, 432–444 (2021).
- Huck, C. J. & Sarlah, D. Shaping molecular landscapes: recent advances, opportunities, and challenges in dearomatization. *Chem.* **6**, 1589–1603 (2020).
- Roche, S. P., Tendoung, J.-J. Y. & Tréguier, B. Advances in dearomatization strategies of indoles. *Tetrahedron* **71**, 3549–3591 (2015).
- Zheng, C. & You, S. L. Catalytic asymmetric dearomatization (CADA) reaction-enabled total synthesis of indole-based natural products. *Nat. Prod. Rep.* **36**, 1589–1605 (2019).
- Gentry, E. C., Rono, L. J., Hale, M. E., Matsuura, R. & Knowles, R. R. Enantioselective synthesis of pyrroloindolines via noncovalent stabilization of indole radical cations and applications to the synthesis of alkaloid natural products. *J. Am. Chem. Soc.* **140**, 3394–3402 (2018).
- An, J., Zou, Y.-Q., Yang, Q.-Q., Wang, Q. & Xiao, W.-J. Visible light-induced aerobic oxyamidation of indoles: a photocatalytic strategy for the preparation of tetrahydro-5h-indolo[2,3-b]quinolins. *Adv. Synth. Catal.* **355**, 1483–1489 (2013).
- Zhu, M., Zheng, C., Zhang, X. & You, S.-L. Synthesis of cyclobutane-fused angular tetracyclic spiroindolines via visible-light-promoted intramolecular dearomatization of indole derivatives. *J. Am. Chem. Soc.* **141**, 2636–2644 (2019).
- Ma, J. et al. Gadolinium photocatalysis: Dearomative [2+2] cycloaddition/ring-expansion sequence with indoles. *Angew. Chem. Int. Ed.* **59**, 9639–9645 (2020).
- Liu, K. et al. Electrooxidation enables highly regioselective dearomative annulation of indole and benzofuran derivatives. *Nat. Commun.* **11**, <https://doi.org/10.1038/s41467-019-13829-4> (2020).
- Wu, J., Dou, Y., Guillot, R., Cyrille Kouklovsky, C. & Vincent, G. Electrochemical dearomative 2,3-difunctionalization of indoles. *J. Am. Chem. Soc.* **141**, 2832–2837 (2019).
- Zhang, Y. et al. Organophotocatalytic dearomatization of indoles, pyrroles and benzo(thio)furan via a Giese-type transformation. *Commun. Chem.* **4**, 20 (2021). Studies from our group and ref 15.
- Zhang, Y. et al. Photoredox asymmetric nucleophilic dearomatization of indoles with neutral radicals. *ACS Catal.* **11**, 998–1007 (2021).
- Pouységu, L., Deffieux, D. & Quideau, S. Hypervalent iodine-mediated phenol dearomatization in natural product synthesis. *Tetrahedron* **66**, 2235–2261 (2010).

17. Dhineshkumar, J., Samaddar, P. & Prabhu, K. R. A copper catalyzed azidation and peroxidation of β -naphthols via an oxidative dearomatization strategy. *Chem. Commun.* **52**, 11084–11087 (2016).
18. Kulish, K., Boldrini, C., Reis, M. C., Pérez, J. M. & Harutyunyan, S. R. Lewis acid promoted dearomatization of naphthols. *Chem. Eur. J.* **26**, 15843 (2020).
19. Sun, W., Li, G., Hong, L., & Wang, R. Asymmetric dearomatization of phenols. *Org. Biomol. Chem.* 2164–2176 (2016)
20. Zhu, G. et al. Chiral phosphoric acid catalyzed asymmetric oxidative dearomatization of naphthols with quinones. *Org. Lett.* **18**, 5288–5291 (2016).
21. Takamura, M., Funabashi, K., Kanai, M. & Shibasaki, M. Asymmetric Reissert-type reaction promoted by bifunctional catalyst. *J. Am. Chem. Soc.* **122**, 6327–6328 (2000).
22. Zurro, M., Asmus, S., Beckendorf, S., Mück-Lichtenfeld, C. & Manchego, O. G. Chiral helical oligotriazoles: new class of anion-binding catalysts for the asymmetric dearomatization of electron-deficient *N*-heteroarenes. *J. Am. Chem. Soc.* **136**, 13999–14002 (2014).
23. Pappoppula, M., Cardoso, F. S. P., Garrett, B. O. & Aponick, A. Enantioselective copper-catalyzed quinoline alkynylation. *Angew. Chem. Int. Ed.* **54**, 15202–15206 (2015).
24. Yan, X., Ge, L., Castiñeira Reis, M. & Harutyunyan, S. R. Nucleophilic dearomatization of *N*-heteroaromatics enabled by Lewis acids and copper catalysis. *J. Am. Chem. Soc.* **142**, 20247–20256 (2020).
25. Leitch, J. A., Rogova, T., Duarte, F. & Dixon, D. J. Dearomative photocatalytic construction of bridged 1,3-diazepanes. *Angew. Chem. Int. Ed.* **59**, 4121–4130 (2020).
26. Ma, J. et al. Photochemical intermolecular dearomative cycloaddition of bicyclic azaarenes with alkenes. *Science* **371**, 1338–1345 (2021).
27. Southgate, E. H., Pospech, J., Fu, J., Holycross, D. R. & Sarlah, D. Dearomative dihydroxylation with arenophiles. *Nat. Chem.* **8**, 922–928 (2016).
28. Okumura, M., Shved, A. S. & Sarlah, D. Palladium-catalyzed dearomative *syn*-1,4-carboamination. *J. Am. Chem. Soc.* **139**, 17787–17790 (2107).
29. Hernandez, L. W., Klöckner, U., Pospech, J., Hauss, L. & Sarlah, D. Nickel-catalyzed dearomative *trans*-1,2-carboamination. *J. Am. Chem. Soc.* **140**, 4503–4507 (2018).
30. Tang, C., Okumura, M., Deng, H. & Sarlah, D. Palladium-catalyzed dearomative *syn*-1,4-oxyamination. *Angew. Chem. Int. Ed.* **58**, 15762–15766 (2019).
31. Wertjes, W. C., Okumura, M. & Sarlah, D. Palladium-catalyzed dearomative *syn*-1,4-diamination. *J. Am. Chem. Soc.* **141**, 163–167 (2019).
32. Siddiqi, Z., Wertjes, W. C. & Sarlah, D. Chemical equivalent of arene monooxygenases: dearomative synthesis of arene oxides and oxepines. *J. Am. Chem. Soc.* **142**, 10125–10131 (2020).
33. Duncton, M. A. J. Minisci reactions: Versatile CH-functionalizations for medicinal chemists. *Med. Chem. Commun.* **2**, 1135–1161 (2011).
34. Proctor, R. S. J. & Phipps, R. J. Recent advances in Minisci-type reactions. *Angew. Chem. Int. Ed.* **58**, 13666–13699 (2019).
35. Romero, N. A., Margrey, K. A., Tay, N. E. & Nicewicz, D. A. Site-selective arene C-H amination via photoredox catalysis. *Science* **349**, 1326–1330 (2015).
36. Margrey, K. A., McManus, J. B., Bonazzi, S., Zecri, F. & Nicewicz, D. A. Predictive model for site-selective aryl and heteroaryl C-H functionalization via organic photoredox catalysis. *J. Am. Chem. Soc.* **139**, 11288–11299 (2017).
37. McManus, J. B. & Nicewicz, D. A. Direct C–H cyanation of arenes via organic photoredox catalysis. *J. Am. Chem. Soc.* **139**, 2880–2883 (2017).
38. Margrey, K. A., Levens, A. & Nicewicz, D. A. Direct aryl C–H amination with primary amines using organic photoredox catalysis. *Angew. Chem. Int. Ed.* **56**, 15644–15648 (2017).
39. Huang, H. et al. Electrophotocatalysis with a trisaminocyclopropenium radical dication. *Angew. Chem. Int. Ed.* **58**, 13318–13322 (2019).
40. Zhang, L. et al. Photoelectrocatalytic arene C–H amination. *Nat. Catal.* **2**, 366–373 (2019).
41. Targos, K., Williams, O. P. & Wickens, Z. K. Unveiling Potent Photooxidation Behavior of Catalytic Photoreductants. *J. Am. Chem. Soc.* **143**, 4125–4132 (2021).
42. Newcomb, M., Choi, S.-Y. & Horner, J. H. Adjusting the Top End of the Alkyl Radical Kinetic Scale. Laser Flash Photolysis Calibrations of Fast Radical Clocks and Rate Constants for Reactions of Benzeneselenol. *J. Org. Chem.* **64**, 1225–1231 (1999).
43. Newcomb, M., Varick, T. R., Ha, C., Manek, M. B. & Yue, X. Picosecond radical kinetics. Rate constants for reaction of benzeneselenol with primary alkyl radicals and calibration of the 6-cyano-5-hexenyl radical cyclization. *J. Am. Chem. Soc.* **114**, 8158–8163 (1992).
44. Yasuda, M., Yamashita, T., Shima, K. & Pac, C. Photochemical reactions of aromatic compounds. 43. Direct photoamination of arenes with ammonia and primary amines in the presence of electron acceptors. *J. Org. Chem.* **51**, 753–759 (1987).
45. Yasuda, M., Matsuzaki, Y., Shima, K. & Pac, C. Photochemical reactions of aromatic compounds. Part 44. Mechanisms for direct photoamination of arenes with ammonia and amines in the presence of *m*-dicyanobenzene. *J. Chem. Soc., Perkin. Trans.* **2**, 745 (1988).
46. Yasuda, M., Watanabe, Y., Tanabe, K. & Shima, K. Regiochemistry on photoamination of methoxy-substituted phenanthrenes via electron transfer. *J. Photochem. Photobiol. A: Chem.* **79**, 61–65 (1994).
47. Mizuno, K., Pac, C. & Sakura, H. Photochemical cyanation of aromatic hydrocarbons with cyanide anion. *J. Chem. Soc. Chem. Commun.* 553 (1972).
48. Xuan, J., Zhang, Z.-G. & Xiao, W.-J. Visible-light-induced decarboxylative functionalization of carboxylic acids and their derivatives. *Angew. Chem. Int. Ed.* **54**, 15632–15641 (2015).
49. Plutschack, M. B., Pieber, B., Gilmore, K. & Seeberger, P. H. The Hitchhiker’s guide to flow chemistry. *Chem. Rev.* **17**, 11796–11893 (2017).
50. Rodgers, J. D., et al. Heteroaryl substituted pyrrolo[2,3-*b*]pyridines and pyrrolo[2,3-*b*]pyrimidines as Janus kinase inhibitors. US2009181959A1.
51. Schirok, H., et al. Substituted 2-amino-pyrazolyl-[1,2,4]triazolo[1,5A]pyridine derivatives and use thereof. WO 2020/215094.
52. Mayer, J. M. Understanding hydrogen atom transfer: from bond strengths to Marcus theory. *Acc. Chem. Res.* **44**, 36–46 (2011).

Acknowledgements

W.W. acknowledges the NIH (5R01GM125920) and University of Arizona for financial support and the NSF MRI for acquisition of 500 MHz NMR spectrometer (1920234). S.C. is grateful to Oberlin College for financial support. K.N.H. thanks the National Science Foundation (Grant CHE-1764328). DFT calculations were performed using the SCIURus, the Oberlin College HPC cluster (NSF MRI 1427949).

Author contributions

P.J., F.G., J.C., and X.M. conducted and analyzed the synthetic experiments. C.C.D. performed DFT calculations under the direction of S.C. K.N.H. and W.W. planned, designed and directed the project. P.J., S.C., K.N.H. and W.W. wrote the manuscript.

Competing interests

The authors declare no competing interests.

Additional information

Supplementary information The online version contains supplementary material available at <https://doi.org/10.1038/s41467-022-32201-7>.

Correspondence and requests for materials should be addressed to Kendall N. Houk, Shuming Chen or Wei Wang.

Peer review information *Nature Communications* thanks Lisa Roy, and the other, anonymous, reviewer for their contribution to the peer review of this work.

Reprints and permission information is available at <http://www.nature.com/reprints>

Publisher's note Springer Nature remains neutral with regard to jurisdictional claims in published maps and institutional affiliations.

Open Access This article is licensed under a Creative Commons Attribution 4.0 International License, which permits use, sharing, adaptation, distribution and reproduction in any medium or format, as long as you give appropriate credit to the original author(s) and the source, provide a link to the Creative Commons license, and indicate if changes were made. The images or other third party material in this article are included in the article's Creative Commons license, unless indicated otherwise in a credit line to the material. If material is not included in the article's Creative Commons license and your intended use is not permitted by statutory regulation or exceeds the permitted use, you will need to obtain permission directly from the copyright holder. To view a copy of this license, visit <http://creativecommons.org/licenses/by/4.0/>.

© The Author(s) 2022